Journal of Power Sources 269 (2014) 825–833

Contents lists available at ScienceDirect

Journal of Power Sources

journal homepage: www.elsevier.com/locate/jpowsour

An O_2 transport study in porous materials within the Li–O_2 – system

Thomas Schied [a, c, d, *], Helmut Ehrenberg [c, d, e], Jürgen Eckert [a, b], Steffen Oswald [a], Martin Hoffmann [a, b], Frieder Scheiba [a, d, e]

[a] IFW Dresden, Institute for Complex Materials, D-01171 Dresden, Germany
[b] Technische Universität Dresden, Institute for Material Science, D-01062 Dresden, Germany
[c] Technische Universität Darmstadt, Material Science, Alarich-Weiss-Straße 2, D-64287 Darmstadt, Germany
[d] Helmholtz-Institute Ulm for Electrochemical Energy Storage (HIU), P.O. Box 3640, D-76021 Karlsruhe, Germany
[e] Karlsruhe Institute of Technology (KIT), Institute for Applied Materials-Energy Storage Systems (IAM-ESS), Hermann-von-Helmholtz-Platz 1, D-76344 Eggenstein-Leopoldshafen, Germany

HIGHLIGHTS

- We give a description of an adaptive experimental Li–O_2 – cell setup.
- Regular and fuel-cell – like O_2 – supply is possible, setup not restricted to Li–O_2.
- Chronoamperometry mandatory to investigate O_2-transport and absorption behaviour.
- Active setup turns out disadvantageous due to unfavourable O_2 flow distribution.
- Simplified strategy to estimate O_2 – absorption, including application on data.

ARTICLE INFO

Article history:
Received 17 April 2014
Received in revised form
8 July 2014
Accepted 11 July 2014
Available online 19 July 2014

Keywords:
Lithium
Oxygen
Active
Transport
Flow
Absorption

ABSTRACT

The research on lithium–oxygen batteries faces a number of issues ranging from design problems to elementary reaction kinetics. Depending on solvent, lithium salt and electrode materials several chemical reaction pathways of lithium and oxygen have been proposed. Oxygen solubility and transport are among the most pressing issues that limit the battery performance. In this work purging oxygen through an electrolyte soaked gas diffusion layer (GDL) was investigated as a possible route towards improving the availability of oxygen to the cell reaction. Additionally based on the findings, a method to estimating the absorption constant of oxygen into the electrolyte is proposed.

1. Introduction

The Li–O_2 electrochemical couple is a candidate for future energy storage systems because of its high theoretical energy density. Its feasibility as a 2nd type battery was shown first by Abraham and Jiang in 1996 [1]. Recently Bruce et al. discovered a highly reversible cell reaction at gold electrodes using 0.1 M $LiClO_4$ in dimethyl sulfoxide (DMSO) solvent [2]. On recharge, the primary discharge product lithium peroxide (Li_2O_2) can be oxidized to retain lithium and oxygen (O_2) – oxygen evolution reaction (OER) – respectively [3], which makes the lithium–air-battery (LAB) interesting for mobile applications. Similar to the commercially available zinc-oxide battery the LAB's concept is to draw O_2 from ambient gas (air or pure O_2) into a porous cathode where the gas is absorbed into the electrolyte. During discharge the O_2 gets reduced – oxygen reduction reaction (ORR) – at the interface between electrolyte and cathode. Subsequently lithium oxides are formed with the lithium coming from the anode side. The thermodynamic cell potentials of Li_2O_2 (2.96 V vs. Li^+/Li) [4a] and lithium oxide (Li_2O) (2.91 V vs. Li^+/Li) [4b] are close to one another. As discharge product in Li–O_2 – cells mainly lithium peroxide (Li_2O_2) [5,6] is reported but also formation of lithium oxide (Li_2O) by further reduction of Li_2O_2 was observed [7]. Consistently two single-electron steps were

* Corresponding author. IFW Dresden, Institute for Complex Materials, D-01171 Dresden, Germany. Tel.: +49 (0)351 4659 1864; fax: +49 351 4659 452.
E-mail addresses: t1001@schied.net, T.Schied@ifw-dresden.de (T. Schied).

http://dx.doi.org/10.1016/j.jpowsour.2014.07.068
0378-7753/

suggested by Hummelshøj et al. in a theoretical work [8]. Alternative to that, a disproportionation reaction was proposed by Laoire and co-workers [9]. The precise reaction path remains however subject of discussion as it is also dependent on the choice of materials and current densities. The formation of Li_2O_2 is kinetically favoured, since it requires the transfer of only 2 electrons compared to 4 electrons for Li_2O. To form 1 mol of Li_2O_2 1 mol of O_2 is required. For 1 mol of Li_2O, only 0.5 mol of O_2 is needed. Hence, O_2 scarcity supports the production of Li_2O, e.g. by reducing existing Li_2O_2.

For the oxygen reduction reaction to occur O_2 and Li ions (i.e. the electrolyte) must be present simultaneously at the electrode surface which acts as an electron donor. This condition of co-existence is frequently referred to as the three-phase-boundary (electrode, electrolyte and gaseous O_2). Therefore, an extension of the three-phase-boundary region was proposed by other groups [7,10,11] to be a route towards higher current densities. However, geometrically a real three-phase-boundary is a line. It would be necessary to rip the electrolyte surface and obtain sufficiently long 3-phase-boundaries to take effect. Since the surface tension of most liquids will prevent this from happening, a slightly different approach is realized in the present work addressing the questions associated with the O_2 transport in Li–O_2 – cells by comparing two different ways of bringing O_2 into the cathode. The classical approach is to expose the cathode material to gaseous O_2 and have the electrolyte absorb it the O_2. Additionally, the cell used for these experiments can be modified to allow for actively purging O_2 through the cathode structure. Active O_2 purging causes a displacement of the electrolyte increasing its surface (beneficial for O_2 absorption) and leaving only a wetting layer on the cathode structure resulting in shorter diffusion paths. Strictly taken, a thin wetting layer is not a 3-phase-boundary but two 2-phase boundaries that are brought close together. The active purging approach is inspired by the typical fuel cell design [12,13]. To the authors knowledge it has not yet been studied for lithium air cells. A potential benefit of the active O_2 enrichment of the electrolyte is connected to the pore clogging issue of high surface cathodes. It is expected that O_2 purging leads to a higher O_2 concentration in deeper regions of a cathode and hence a larger active electrode area. As a consequence the capacity at higher current densities would be improved.

As an electrolyte the ionic liquid (IL) 1-methyl-1-propylpiperidinium bis(trifluoromethylsulfonyl)imide ([PP13][TFSI]) with the lithium salt lithium bis(trifluoromethylsulfonyl) imide (LiTFSI) was chosen. Solvents like carbonates or ethers were not considered due to their higher vapour pressure which leads to a dry out of the cell when it is constantly purged with O_2. In addition, it was found by other research groups, that carbonates and ethers have limited stability in lithium air batteries. Carbonates decompose during discharge [14] as they are unstable against the nucleophilic attack of the superoxide radical [15]. Ethers oxidize on recharge and they may form hydro-peroxides by auto-oxidation [16]. The ionic liquid (IL) [PP13][TFSI] can be an alternative, as it showed good compatibility with carbon in the vicinity of lithium and Li–O products, when used together with LiTFSI [17,18]. The advantages of ILs are typically a very low (negligible) vapour pressure and their hydrophobic nature. Ionic liquids usually have a higher viscosity (slow diffusion) compared to carbonates but they exhibit a rather large potential stability window (1.1 V–5.5 V vs. Li^+/Li in case of [PP13][TFSI]). They are inert with most chemicals as well as non-flammable which makes them promising candidates for future LABs [19]. An additional important fact – as the described experiments are conducted in an open environment – is the low temperature sensitivity of similar RTIL's O_2 solubility as reported by Monaco et al. [20].

This article introduces and discusses the transport and active enrichment of O_2 for Li–O_2 cells as a cornerstone principle to enhance the performance of this type of cell. It is not intended to optimize either flow field geometries or the electrolyte/cathode material compositions or to provide a construction plan. Instead the results presented here serve as an orientation basis for ongoing research into this direction.

2. Experiment

Unless stated differently all Li–O_2 – cells consisted of a metallic lithium anode, a separator and a carbon based porous cathode fully soaked with electrolyte. Subsequently, the cell design and the active components are described. Cell assembling was done in an MBraun Labmaster SP Glove box with H_2O and O_2 level of $\leq$0.6 ppm and <0.1 ppm respectively. Electrochemical investigations were done using a VMP3 potentiostat from BioLogic.

2.1. Cell design

The cell used in the present work comes in a passive and an active (Fig. 1a and b respectively) assembling mode (hollow stamp and channel stamp respectively). The hollow stamp allows exchanging the gas volume above the cathode (e.g. Ar → O_2) without "actively" pushing gas into the cathode structure. In active mode, O_2 is pushed directly through the cathode structure. The active mode stamp is massive but with two channels cut into the surface (Figs. 1b and 3). During the operation one channel (inlet) is fed with a gas (e.g. O_2). To enter the other channel (outlet), the gas has to pass through the cathode structure. The active components are stacked on a height-adapting plate carried by electrically conducting springs. To prevent a short circuit and to keep the plate in its horizontal position a polytetrafluoroethylene (PTFE) spacer is put between the stamp and the plate. The upper shell becomes the positive electrode and vice versa for the lower shell. The stamp for active design is shown from below in Fig. 3. Each channel is accessed through a drilling hole indicated by a black dot. The blocking factor (blocked area over total stamp area) of the active mode channel structure is $\beta = 0.446$.

2.2. Active components

2.2.1. Anode

The anode consists of a 250 μm thin foil of lithium and is used as received from Chemetall without treatment. A Celgard PP/PE/PP

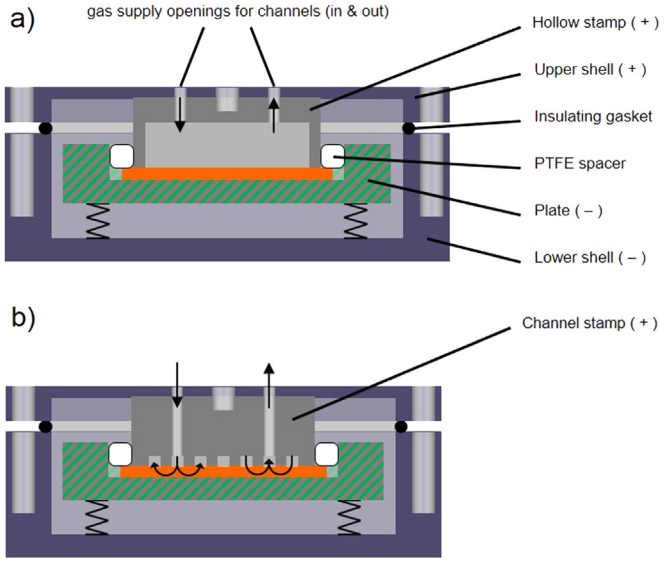

Fig. 1. Sketch of a cross section of the cell in a) passive and b) active mode.

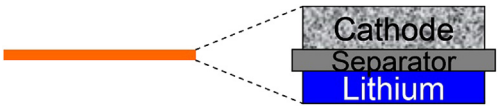

Fig. 2. Active components as arranged on the plate.

Trilayer 2325 (polypropylene PP, polyethylene PE, thickness 25 μm) with a Gurley number of 620 is used as a separator.

2.2.2. Cathode

Commercial gas diffusion layers (GDL) with an optional micro porous layer (MPL) by Freudenberg FCCT KG were used as cathodes (H2315 and H2315 C4). When the GDL-MPL combined cathode was used, it was oriented with the MPL facing the separator and the GDL facing the O_2 side. The GDL is made of a nonwoven fabric of 10 μm thick amorphous carbon fibres (fibres consisting of 96–97% carbon). The specific surface (measured with the Brunauer–Emmett–Teller method – BET) is specified by the manufacturer to be below 0.57 $m^2\ g^{-1}$. From the mass density of the carbon fibres a porosity of 0.787 was calculated. The MPL is made of carbon black containing 80% carbon and 20% PTFE binder. The specific surface of the MPL is 38 $m^2\ g^{-1}$. Before cell assembly the cathodes were put into a vacuum oven at 100 °C for at least 24 h to remove residual moisture. The cathodes were cut to sheets of size 35 × 35 mm^2.

2.2.3. Electrolyte

The electrolyte consisted of the room temperature ionic liquid (RTIL) 1-methyl-1-propylpiperidinium bis(trifluoromethylsufonyl) imide ([PP13][TFSI]) 99% anhydrous from io-li-tec with 0.25 mol L^{-1} of conductive salt LiTFSI (from Aldrich). The salt was dried in a vacuum oven at 100 °C for at least 24 h before usage. To further reduce possible water contamination in the electrolyte, stripes of lithium metal were put into the electrolyte while stirring. When the lithium stripes tarnished, new lithium was added to the electrolyte until tarnishing did not proceed.

2.2.4. Oxygen

The cell was operated in O_2 3.5 (O_2: 99.95%, H_2O: 10 ppmv, Ar: <500 ppmv) as received from Air Liquide.

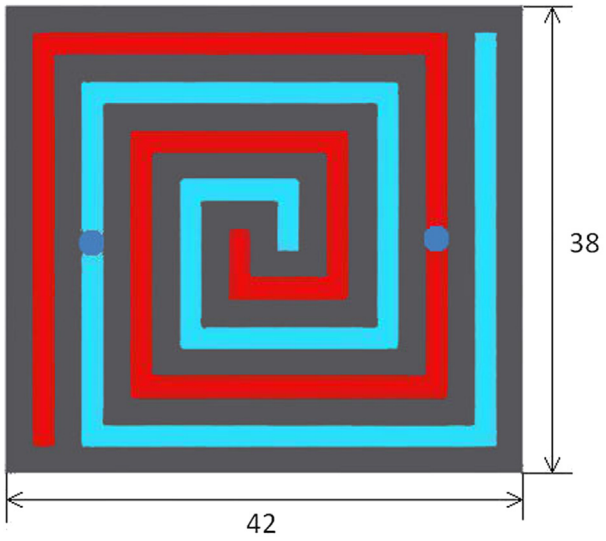

Fig. 3. Active mode stamp with curly channel structure. Inlet (red) and outlet (blue). Dark blue circles indicate the supply/drain for the inlet/outlet channels. (For interpretation of the references to colour in this figure legend, the reader is referred to the web version of this article.)

During cell assembly the active components are arranged onto the steel plate from bottom to top as follows – lithium anode, separator with electrolyte, cathode material – as schematically shown in Fig. 2.

2.3. Methods

To observe the O_2 transport behaviour the reaction of the cells upon discharge is monitored from the moment on where the cathode sees O_2 for the first time. This requirement rules out discharging the cell at constant currents because without O_2 there is no redox couple at the cathode side to account for a current. Using constant current (galvanostatic cycling with potential limitation – GCPL) would either end automatically because of the potential limitation of the potentiostat or cause decomposition of the electrolyte and/or cathode material. Instead a fixed potential is applied to discharge the cell and the current answer is recorded (Chronoamperometry – CA). The potential is applied to the cell before O_2 is supplied. Then, after an equilibration time, O_2 is fed to the cathode. A suitable range of discharge potentials was determined by means of cyclic voltammetry (CV). Discharging was done at fixed potentials ranging from 2.4 down to 2.0 V vs. Li^+/Li until the current dropped near to the base line for a time that was long compared to the time needed to obtain most of the charge. Secondary electron microscope (SEM) pictures were made to track structural changes of the reaction product when the discharge conditions are altered (discharge potential, passive or active mode). All SEM pictures were made with a JEOL JAMP 9500F Scanning Auger Microscope. To avoid sample changes due to influence of air, an Ar filled transfer vessel was used for sample transport from the glove box.

3. Results/discussion

The cells have an open circuit voltage (OCV) of ~2.65 V. This value is lower than the thermodynamically predicted value because the cell lacks a second redox-couple – i.e. O_2^-/O_2 – to develop a stable equilibrium potential until O_2 is first introduced (discharge reaction starts immediately since the cell is polarized to the discharge voltage before O_2 is fed into the cell). Instead, the found voltage of 2.65 V is determined by reactions of surface groups on the carbon electrode (e.g. protolysis reaction of carboxyl groups: $COOH \leftrightarrow COO^- + H^+$). Such reactions usually depend strongly on the choice of electrolyte. The OCV was found to be closer to 3 V for DMSO as well as glymes and carbonates. However, even in the presence of O_2 the OCV value differs from the thermodynamically predicted value of 2.96 V vs. Li^+/Li since the reduction of O_2 in aprotic solvents involves the formation of the highly unstable superoxide (O_2^-) anion and hence is not reversible in the sense of a chemical equilibrium reaction, but also because the O_2 reduction kinetics is very slow.

The cyclic voltammetry measurement (Fig. 4) shows that the discharge reaction starts at a potential around 2.6 V. Upon cycling, the current decays on both discharge and recharge. This decay must be attributed to passivation of the active material due to unresolved reaction products. The scan rate was 5 mV s^{-1} and the decay is seen most clearly near the vertex potentials of the CV.

The cathodic sweep shows an (negative) increasing current that peaks at $E_c \leq 2$ V. The anodic sweep shows no direct corresponding oxidation peak, indicating that none of the reaction products participate in an electrochemically reversible reaction. One of these products could be the intermediate reduction product O_2^- (superoxide radical). It is consumed by a follow up (chemical) reaction which is not reversible in an electrochemical sense. The first reverse process during anodic sweep starts at 2.8 V. Its maximum current is reached at $E_{a1} = 3.3$ V. A second oxidation process is seen

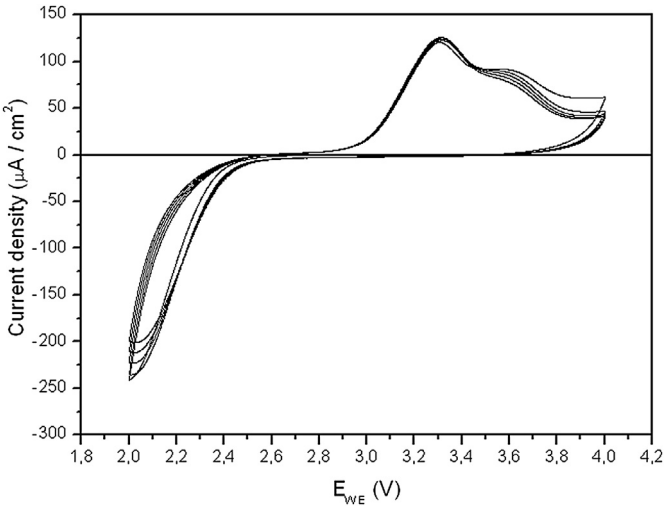

Fig. 4. Cyclic voltammetry at scan rate 5 mV s^{-1} (in O_2 3.5).

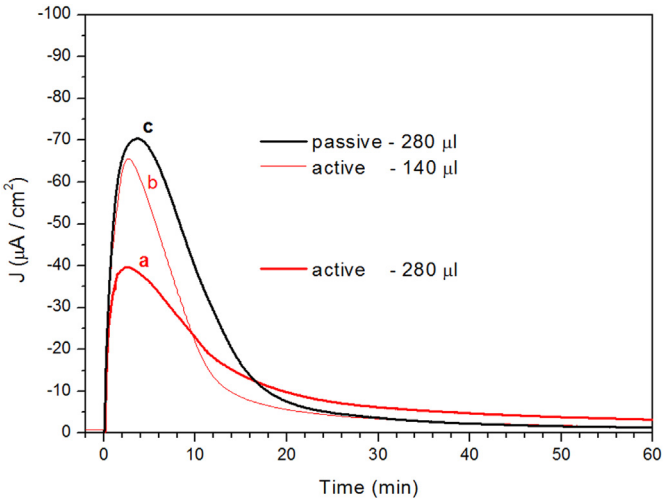

Fig. 5. Cells discharged at 2.2 V vs. Li^+/Li. Cells are discharged in a) active mode fully filled, b) active mode half-filled and c) passive mode fully filled.

at $E_{a2} = 3.6$ V. The anodic sweep of the CV encloses a bigger area (charge) than the cathodic sweep. The presence of two oxidation peaks has been reported before by Trahan et al. [21] although their potential positions have different values depending on the choice of electrolyte. The first oxidation peak was identified to be the direct oxidation of Li_2O_2 and the second one was assigned to the removal of a residual passivation layer which according to Trahan et al. restores the initial behaviour of the material (Trahan et al. used glassy carbon as cathode material and DMSO as a solvent).

For transport measurements the potential range 2.0–2.4 V was chosen because of the continuous current increase in that region of the CV.

3.1. O_2 – Transport

The anion part of the lithium–salt molecules is much bigger than the O_2 – molecule. Accordingly the purely diffusive transport of O_2 is expected to be faster than the transport of lithium – salts. The high lithium – salt concentration however over-compensates the slow transport properties by far. For the same reason Li^+ and $TFSI^-$ migration due to concentration over-potentials is expected to be very low/negligible.

Using the potential step method yields the maximum electrical current that the cell is able to deliver at a particular operating voltage. The delivered current must be attributed to the slowest process in the cell. The *I*–*t*-curve contains information about the processes in the cell including their time scales.

Only the simple model cathodes are regarded. Pure GDLs were used as cathode material and discharged in different O_2 supply modes. The results are shown in Fig. 5. At the beginning the active mode cells' (two red curves a and b in Fig. 5 (in the web version)) performance is lower than the passive mode cell's (black line). The capacity though is roughly preserved, as the current density (active mode) stays high for a few hours more compared to passive case. Therefore it takes longer for the active mode cells to completely discharge which indicates, that the O_2 supply in passive mode is faster than in active mode. The limited current density must be attributed to a lower O_2 concentration in active mode since, apart from the way O_2 is supplied, other environment variables remained equal.

In passive mode, the cathode was filled completely with electrolyte. The discharge curve of a half filled passive mode cell does minimally deviate from the fully filled one. It is not shown here. The fully filled active mode cell has the least performance as shown in Fig. 5. Since the reason for this behaviour must be related to transport, an active mode cell with half the amount of electrolyte was assembled and showed a higher performance which supports the idea that the passage of O_2 through the fully filled cathode structure is hindered in active mode and becomes easier in a half filled cell - where there is less electrolyte left to displace. However, the overall capacity of the half-filled cell is reduced.

In order for the O_2 gas to pass through the filled cathode it must displace a portion of the electrolyte according to its flow rate. The displacement of electrolyte is connected with an increase of electrolyte surface. The surface energy of the electrolyte is however trying to minimize the electrolyte's surface area. It is therefore unlikely for the electrolyte to be displaced homogeneously along the inlet channel to allow for a homogeneous O_2 flow along the inlet channel. Instead the electrolyte will be displaced inhomogeneously. According to the Plateau-Rayleigh – Instability, somewhere along the inlet channel a small rip of the electrolyte will occur and grow towards a lower pressure region. It will form a gas path which will result in a shortcut between inlet and outlet channel. The size of this shortcut path will be only as large as the surface energy allows for. The shortcut allows O_2 to flow into the outlet channel causing a pressure drop in the inlet channel. Electrolyte will stop being displaced further and most of the O_2 passes through the shortcut path to the outlet channel. This process leads to an inhomogeneous O_2 – distribution and corrupts the fast delivery of O_2 to all parts of the cathode. The channel structure itself prevents more than 50% of the cathode top layer to get into direct contact with O_2 (blocking factor $\approx$ 0.45). Additionally only one channel (of two) is purged with O_2. A scheme of this process is shown in Fig. 6. The maximum current of the fully filled active cell as well as the electrical charge up to 20 min (when the main current peak is passed) equal about 60% of the respective quantities in the passive case. This percentage exceeds the value suggested by the blocking factor (45%) because this factor does not take into account O_2 reaching a yet larger region by diffusion. Eventually O_2 will slowly (e.g. lateral diffusion and by slowly removing residual Argon from the channels) distribute among the cathode. Regarding the spatial average the O_2 concentration is lower than in passive mode as not all of the cathode surface is directly exposed to O_2. However, locally the O_2 concentration will be even higher than in passive mode, e.g. where the shortcut forms. The performance of the half-

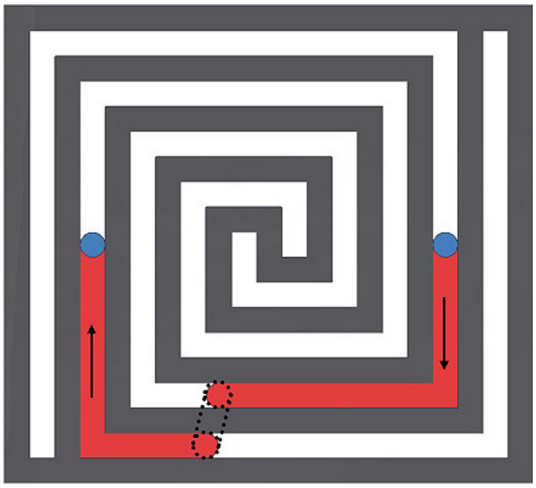

Fig. 6. Shortcut gas path in active mode (O_2 indicated by red colour). (For interpretation of the references to colour in this figure legend, the reader is referred to the web version of this article.)

filled active mode cell is better because a half filled cathode structure leaves more open space for O_2 flow to penetrate the cathode structure, allowing a more homogeneous O_2 distribution with less electrolyte to be displaced.

Because of its performance advantage the passive mode was investigated more closely. Cells were discharged at different potentials (Fig. 7). Curve c) of Fig. 7 is the passive mode discharge curve known as curve c) from Fig. 5 (Scale is changed). The other cells a), b) and d) were discharged at 2.4 V, 2.3 V and 2.0 V respectively.

The performance of a cell is governed by O_2 reduction kinetics, absorption rate and diffusion rate, one of which is always the limiting process. The reduction kinetics can be influenced via over-potential. As expected, a higher over-potential causes a higher consumption rate of O_2 and thus higher maximum current. The corresponding discharge curves are included in Fig. 7. The capacity does increase with higher over potential. This indicates that a larger potential difference on the electrode-electrolyte interface leads to a higher electron tunnelling probability and allows the Li_2O_2 deposits to grow thicker. Judging from these results up to 2.0 V the reaction kinetics is the main limiting process in passive mode for these cathodes. As long as the O_2 − supply is fast enough, a higher over potential can cause higher currents.

When a very cathodic potential is applied (reduction kinetics is fast), other processes become rate limiting. A candidate process is the absorption rate of O_2 by the electrolyte. A first indication was found in Fig. 5. In active mode, a part of the cathode is covered by the channel walls (blocked) and will thus not come into direct contact with O_2 (only a fraction of the electrolyte surface is exposed to O_2). Hence, a smaller amount of O_2 is absorbed into the electrolyte per unit time, causing a performance decrease. To further support this reasoning two more active mode cells were discharged at lower potentials, analogous to the passive mode cells in Fig. 7. The curves in Fig. 8 show, that in active mode the supply of O_2 must have run into a limit. Comparing the active discharge curves taken at the potentials 2.2 V and 2.0 V in Fig. 8 we find that the under-supply of O_2 causes the maximum current to decrease rapidly after peaking. Increasing the over voltage in active case does shortly improve the current density but a lower O_2 absorption leads to a more rapid decrease than in an equivalent passive mode measurement at 2.0 V (cf. Fig. 7d).

The afore used cathodes have a very low specific surface of only about 0.57 $m^2\ g^{-1}$. Due to their high porosity these cathodes do not efficiently use the O_2 present in the electrolyte. To show this, similar cathodes with an additional micro porous layer (MPL) on one side were used and measured analogously to the passive mode GDL series (discharged at 2.4 V, 2.2 V and 2.0 V). The results are shown in Fig. 9. Higher current densities and discharge capacities are achieved by using this cathode material with a higher specific surface. The high rate curves have two maxima reflecting the 2-layer composition of the cathode. At low rate the second maximum is not so prominent. Because of the lower O_2 consumption rate in the GDL part of the cathode O_2 reaches the MPL part earlier thus bringing the two maxima closer together. They appear merged at 2.4 V discharge. At high rate, more O_2 is used in the front region of the cathode (giving the first maximum) before O_2 can reach deeper parts of the cathode, where a second maximum shows up. Compared to the pure GDL cathodes, the first maximum here has a much higher current density. This can only be explained if some of the O_2 is actually reaching parts of the MPL right from the start, which can happen in two ways. One is, that O_2 bypasses the GDL layer at the sides of the cathode and thus gets into contact with the side region of the MPL. The second way is caused

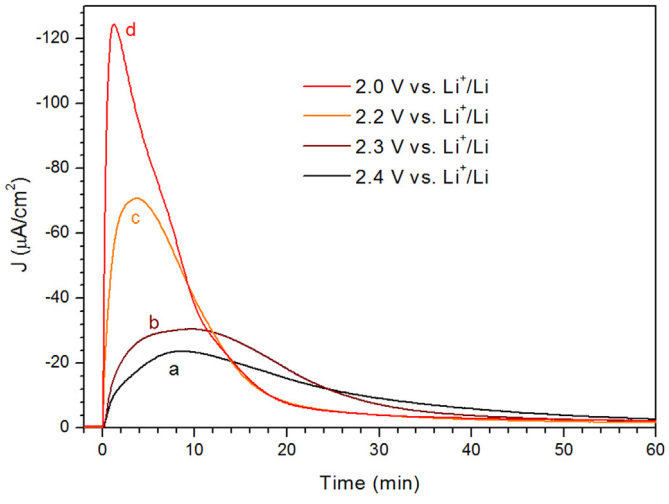

Fig. 7. Passive mode GDL cells discharged at a) 2.4 V, b) 2.3 V, c) 2.2 V and d) 2.0 V vs. Li^+/Li.

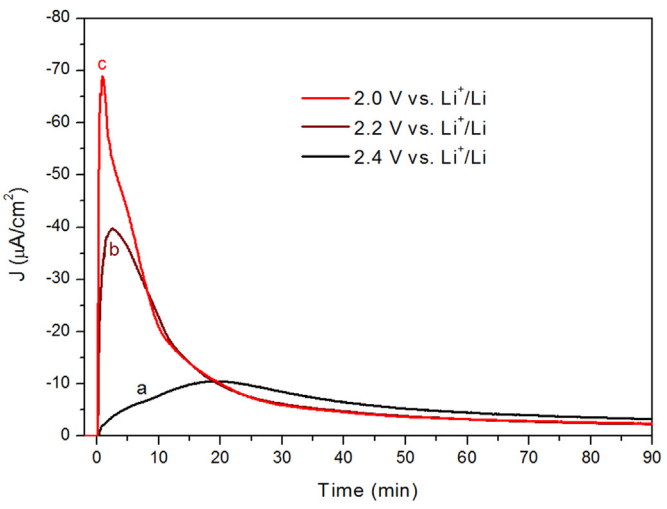

Fig. 8. Active mode GDL cells discharged at a) 2.4 V, b) 2.2 V and c) 2.0 V vs. Li^+/Li.

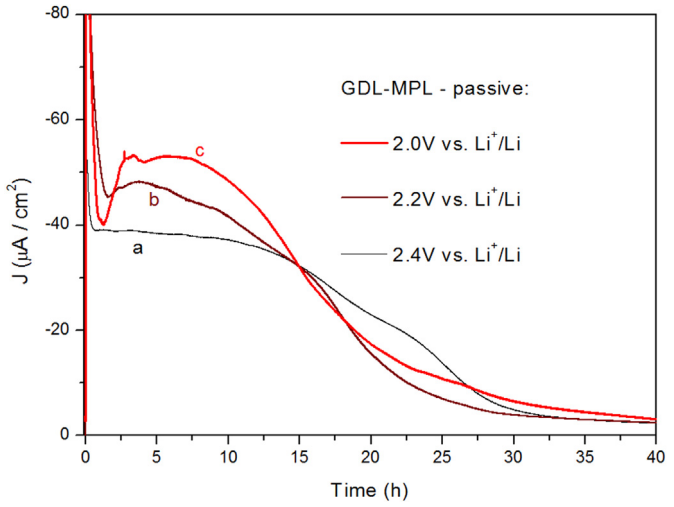

Fig. 9. Passive mode MPL cells discharged at a) 2.4 V, b) 2.2 V and c) 2.0 V vs. Li^+/Li.

by the way the 2-layer cathode is assembled. There is no sharp border between the GDL part and the MPL part. Instead some of the C-fibre in the rear part of the GDL are surrounded by MPL material to attach the MPL to the GDL. This thin transition region facilitates the entering of O_2 into the MPL material, combining high area (from MPL) with high porosity (from GDL). The transition region between cathode layers is shown in Fig. 10. Because of the high porosity the transition region is reached by O_2 quickly, so it contributes significantly to the initial current density (increasing the first maximum).

3.2. SEM investigation

Changing the discharge potential caused a slightly higher capacity which raises the question for the morphology of the discharge products. In Fig. 11 cathodes discharged in passive and active mode are shown. In passive mode the reaction product appears to form flat flake like islands. At 2.0 V a higher island density than at 2.2 V is found. The islands at 2.0 V even start to form a closed layer of reaction product whereas at 2.2 V the islands appear to be more separated. The active mode cells exhibit, however, a slightly different morphology. Optically the islands appear less flat, and their average spatial density is much lower due to the reduced capacity compared to passive mode cells. These findings support the conclusion that the average O_2 concentration is reduced in active mode and furthermore, that it is energetically favourable for islands to grow larger instead of nucleating under O_2 scarcity conditions.

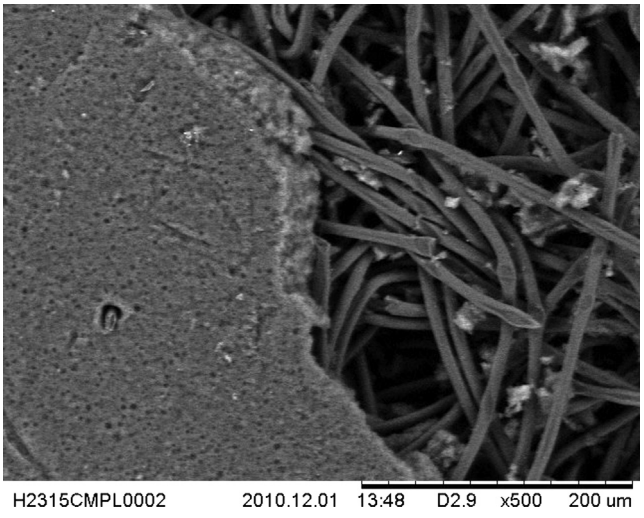

Fig. 10. Transition region between MPL (left) and GDL (right), about 10 µm thin.

3.3. Flow rate dependence

Since the flow rate is an environmental variable it is likely to influence the cell performance. To point out the performance sensitivity to the flow rate, cells were measured at 2 ml min^{-1} and 20 ml min^{-1} additionally to the 10 ml min^{-1} already shown in Fig. 7. The discharge potential of $E = 2.2$ V was applied to the new cells. The results are shown in Fig. 12. A higher flow rate causes a higher O_2 absorption rate (due to faster growing O_2 partial pressure) which then causes a higher O_2 concentration and hence a larger peak current density. Another effect of the accelerated absorption is that the current density also increases faster which also accelerates the cathode passivation. Therefore the maximum current density is reached earlier and the current density peak shifts to an earlier time. Lowering the O_2 flow rate has the exact contrary effect.

3.4. Absorption constant

The O_2 absorption behaviour is one potentially limiting process. In this section we introduce an evaluation technique that could be used to estimate the O_2 (or another gas) absorption constant of a system. Only the first seconds of the discharge curve can be used for this evaluation. As a precondition the respective gas (O_2) saturation concentration must be known (Henry's constant) and the following assumptions are made:

1) The O_2 concentration is very low at the beginning. Hence, O_2 that reaches the surface of the foremost region of the cathode is instantly consumed (this does not hold true for all times since O_2 also diffuses into the cathode)
2) The integrated measured current (charge) is directly proportional to the amount of O_2, absorbed into the electrolyte
3) Surface passivation by reaction products is negligible (due to low O_2 concentration).

These assumptions lead to the simple expression, that the measured current I is proportional to the absorption rate J (substance flux):

$$I \sim J_{\mathrm{abs}} \tag{1}$$

Expressing this fact differently, the amount of charge is proportional to the amount of substance of O_2 that is absorbed. Faraday's constant relates the electrical charge to a certain number of electrons. To form one Li_2O_2 two electrons are required, so the O_2 amount must be half the amount of electrons:

$$\frac{C(t)}{F} = n_{e^-}(t) = 2 \cdot n_{O_2}(t) \tag{2}$$

The charge is obtained by time integration of the measured current.

$$C(t) = \int_0^t I(t') \cdot \mathrm{d}t' \tag{3}$$

Oxygen absorption can be defined by a volume of gas being absorbed through an area during a certain time.

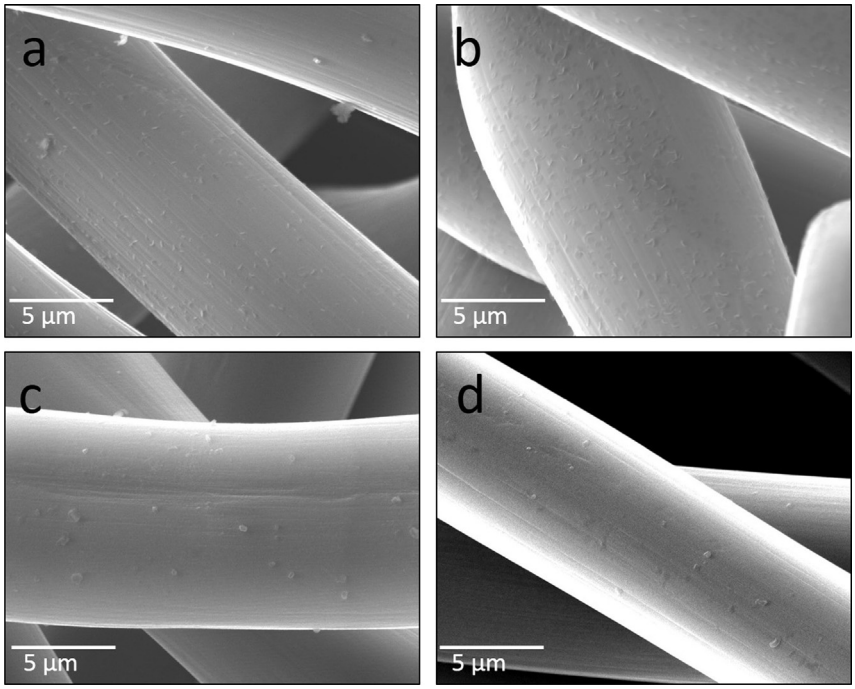

Fig. 11. SEM pictures of GDLs discharged in passive mode at a) 2.2 V and b) 2.0 V as well as in active mode at c) 2.2 V and d) 2.0 V.

$$V_{abs} = \alpha \cdot A_{abs} \cdot t_{abs} \tag{4}$$

According to these expressions the absorption constant α has the dimension $[\alpha] = \text{m s}^{-1}$. Another definition of the absorption constant relates the O_2 absorption (molar) flux to a concentration difference [22]. The concentration difference is made up of the actual O_2 concentration in the foremost region of the cathode (which is exposed to O_2) and the equilibrium O_2 concentration according to Henry's law.

$$-D\frac{\partial c}{\partial x}\bigg|_{x=0} = J_0 = \alpha \cdot (c_{O_2,eq} - c_0) \tag{5}$$

D is the diffusion coefficient, c_0 the O_2 concentration at the O_2 side and x the spatial parameter. For the first seconds c_0 can be assumed to be zero, $c_0 = 0$. According to Henry's law the equilibrium concentration is:

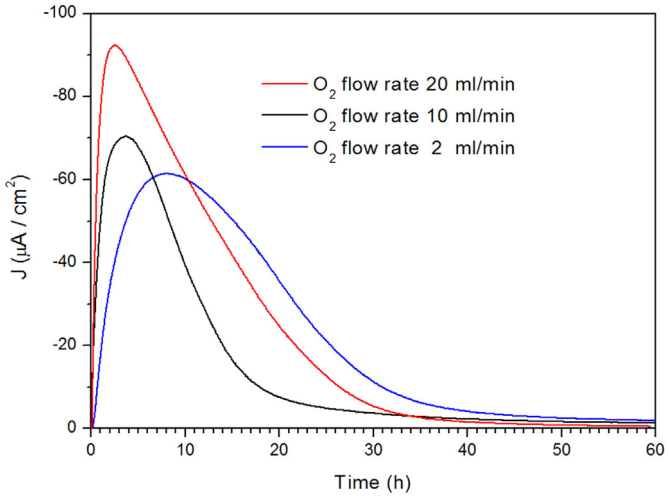

Fig. 12. Transport measurements: performance sensitivity on O_2 flow rate.

$$c_{O_2,eqn} = k_{H,cp} \cdot p \tag{6}$$

Here, $k_{H,cp}$ is the Henry – coefficient of O_2 solubility. The O_2 flux into the cell is controlled by a mass flow device, so equation (7) describing the O_2 partial pressure p above the cathode can be derived assuming homogeneous mixing of Ar and O_2.

$$p(t) = p_0 \cdot \left(1 - e^{-\frac{R}{V} \cdot t}\right) \tag{7}$$

Here p_0 is the ambient pressure, R is the flow rate of O_2 and V is the void volume above the cathode (in which Ar left from assembling in the glove box is replaced by O_2). The flux of a species (O_2) is defined as the amount of substance n_{O_2} passing through a certain geometric area A_{geom} in a time t:

$$J = \frac{n_{O_2}}{A_{geom} \cdot t} \tag{8}$$

Combining the equations (2), (3) and (5–8) yields the absorption constant α, which firstly is a function of time. An arithmetic average value can be calculated.

$$\alpha(t) = \frac{C(t)}{2 \cdot F \cdot A_{geom} \cdot k_{H,cp} \cdot p_0} \cdot \frac{1}{t \cdot \left(1 - e^{-\frac{R}{V} \cdot t}\right)} \tag{9}$$

Finally one has to consider the porosity of the cathode again. In the present case, the material used has a porosity of ~78%. The more dense (less porous) a material is, the faster O_2 will reach a surface to participate in a reaction. With porosity 100% (no material), no reaction will occur, whereas with porosity 0% all of the gas would react instantly on the surface of the material. Assuming a linear transition between these two extreme cases the calculated absorption constant α is regarded as a "real" absorption constant α_r being fudged (i.e. multiplied) by the volume fraction v_{cath} (here $v_{cath} = 0.213$) of the porous material, accounting for the porosity in this way:

$$\alpha = \alpha_r \cdot v_{\text{cath}} \tag{10}$$

Evaluation of α_r from passive mode curves (cf. Fig. 7):

As the O_2 solubility of the RTIL used in the present experiments is not known, reported values from the RTIL [bmim][PF_6] were taken instead. Generally the viscosity of a medium is a measure for the interaction strength of its molecules. Thus, in a certain range the solubility for a species (e.g. O_2) should increase, the weaker the solvent's self interaction is. The physical properties of [bmim][PF_6] (density, viscosity) are comparable to the RTIL used in the present experiments, as shown in Table 1. The cations of the RTILs differ only by one of their alkyl groups (propyl ↔ butyl). The anion part of [bmim][PF_6] has a higher symmetry then the $TFSI^-$ anion in [PP13][TFSI]. Apart from self interaction, this might be another factor for the higher viscosity of [bmim][PF_6].

The O_2 solubility of [bmim][PF_6] is given in terms of the Henry constant $k_{H,cp} = 0.0026$ mol $(atm \cdot l)^{-1}$ [23]. Since the viscosity of [bmim][PF_6] is larger than that of [PP13][TFSI] it is reasonable to expect the O_2 solubility of [PP13][TFSI] to be higher than in [bmim][PF_6]. However, no linear relation can be expected between O_2 solubility and viscosity. Currently a simplified computer model is developed to aid in refining the value of the Henry constant to account for the behaviour of [PP13][TFSI]. Recent calculations point towards a value of the Henry's constant of $k_{H,cp} \approx 0.07$ mol $(atm \cdot l)^{-1}$, supporting the argument above. The results of the model calculations help to evaluate the accuracy of the estimated absorption values in this article. The model itself and its results are not subject of this publication. Using the calculated value of $k_{H,cp} = 0.07$ mol $(atm \cdot l)^{-1}$, the "time dependent" absorption constant α_r is calculated for the first 10 s of discharge under O_2. The result is shown in Fig. 13.

Although the value of the absorption constant should not be depending on the discharge rate large differences between the absorption constants are found at different discharge rates (i.e. potentials). A general flaw of this evaluation method is that it does not explicitly consider the effect of the discharge rate. The absorption constant seems to increase with the discharge rate. Instead the most suitable data set for estimating the absorption constant is identified considering the following:

The absorption rate of O_2 is limited by the liquid's transport properties. Slow transport makes the surface region of the electrolyte saturate faster with O_2. The surface is then blocked for further absorption. The CV in Fig. 4 shows a peaking of the current density close to 2.0 V. Here the current starts to become transport controlled. The 2.0 V discharge data are most suitable to estimate the absorption constant because it causes the highest possible consumption rate of O_2. Since at the very beginning of the discharge most of the O_2 is consumed in the surface near region, the diffusion paths of O_2 are very short, so that diffusion plays only a minor role, leaving the absorption as the main limiting process. This allows to draw conclusions about the absorption by evaluation of the current in the very first seconds of the discharge.

Table 1
Densities and viscosities of RTILs PP13TFSI and [bmim][PF_6]. Values for [bmim][PF_6] were extrapolated based on the data provided by Qiao et al. [23] Data about PP13TFSI was taken from supplier iolitec.

Ionic liquid	Density ρ (g cm^{-3})	Viscosity η (mPa s)	Ref.
PP13TFSI	1.4	169.8	Iolitec
[bmim][PF_6]	~1.368	~220	Qiao et al. [23]

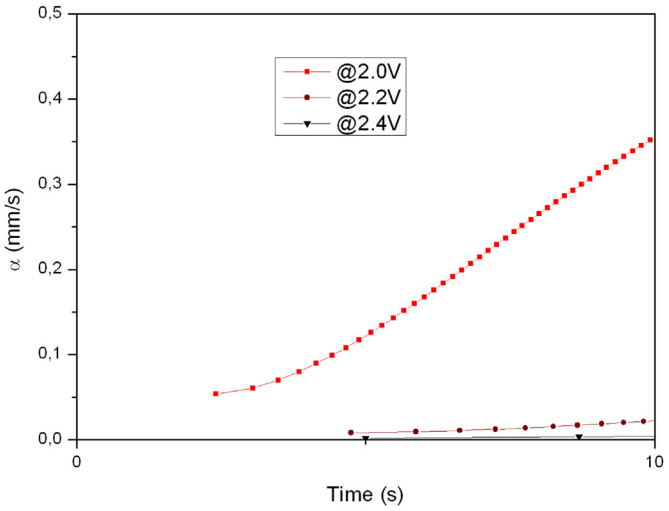

Fig. 13. Absorption constant α calculated from discharge curves (@ 2.4 V, 2.2 V, 2.0 V).

Taking the averaged value of the first 10 s a value of $\alpha = (0.21 \pm 0.09)$ mm s^{-1} is found. The proposed method might allows to estimate the order of magnitude of α. However, the extensive simplifications in this method require caution.

4. Conclusions and outlook

The active enrichment of the electrolyte with O_2 leads to performance loss. Due to inconvenient fluid dynamics of the ionic liquid based electrolyte the O_2 distribution over the cathode structure is non-homogeneous compared to passive mode. The non-homogeneity leaves parts of the cathode free of O_2. In this experimental setup the passive mode approach remains the more effective way to feed O_2 to the Li–O_2 cell.

The comparison of cells in passive and active mode, discharged at different potentials showed that in passive mode the discharge potential can be used to increase the O_2 consumption rate (and thus current density) to a certain extend. In active mode an O_2 transport limitation seems to intervene before current densities similar to passive mode are reached. The capacity increases when cells are discharged at more cathodic potentials which is attributed to the larger potential difference across the cathode/electrolyte interface and aids in growing thicker lithium oxide layers. In addition a partial reduction of Li_2O_2 to Li_2O may also contribute to the increased capacity.

To improve the O_2 enrichment in Li–O_2 cells a way has to be found to circumvent the inhomogeneous O_2 flow through the cathode structure and avoid O_2 pressure breakdown due to shortcuts. We propose the usage of a different electrolyte type such as solid state or polymer (similar to fuel cells). Other than liquid electrolytes, solid state or polymer electrolytes can maintain an open pore structure to allow for the O_2 flow to occur more readily and homogeneous.

Connected to the measurement technique used to obtain the present results, a simplified evaluation method is established to estimate the order of magnitude of the absorption rate constant α of the electrolyte if the saturation concentration (Henry constant) of the active gas (here O_2) is known for the respective electrolyte.

Apart from the disadvantages regarding Li–O_2 cells the introduced cell design offers practical possibilities such as controlled feeding of substances to a cell to influence the chemical reactions, purging gases or fluids through the cell, which could be particularly interesting for aqueous systems (on the

cathode side). Gas analysis can be done easily by closing the outlet, storing evolving gases in the cell and flushing them out to an analyzing device using a carrier gas such as Argon. Additionally the system can be extended to allow for pressure or temperature measurements.

Acknowledgement

Financial support from the DFG Research Collaborative Center SFB 595 (Electrical fatigue in functional materials) is gratefully acknowledged.

Special thanks go to M. Uhlemann who helped in assembling the peripheral instruments for O_2-supply as well as in eliminating leaks of the prototype cells at the beginning of the experiments. Further thanks go to M. Klose for providing BET data and S. Kaschube for SEM pictures.

References

[1] K.M. Abraham, Z. Jiang, J. Electrochem. Soc. 143 (1996) 1–5.
[2] Z. Peng, S.A. Freunberger, Y. Chen, P.G. Bruce, Science 337 (2012) 563–566.
[3] T. Ogasawara, A. Débart, Holzapfel, P. Novák, P.G. Bruce, J. Am. Chem. Soc. 128 (2006) 1390–1393.
[4] M.W. Chase Jr., J. Phys. Chem. Ref. Data, Monogr. 9 (1998). NIST-JANAF Thermochemical Tables: (a) p. 1510; (b) p. 1506.
[5] A. Debart, A.J. Paterson, J. Bao, P.G. Bruce, Angew. Chem. Int. Ed. 47 (2008) 4521–4524.
[6] J. Read, J. Electrochem. Soc. 149 (2002) A1190–A1195.
[7] S.S. Zhang, D. Foster, J. Read, J. Power Sources 195 (2009) 1235–1240.
[8] J.S. Hummelshøj, J. Blomqvist, S. Datta, T. Vegge, J. Rossmeisl, K.S. Thygesen, A.C. Luntz, K.W. Jacobsen, J.K. Nørskov, J. Chem. Phys. 132 (2010) 071101.
[9] C.O. Laoire, S. Mukerjee, K.M. Abraham, E.J. Plichta, M.A. Hendrickson, J. Phys. Chem. C 113 (2009) 20127–20134.
[10] A. Kraytsberg, Y. Ein-Eli, J. Power Sources 196 (2011) 886–893.
[11] R. Padbury, X. Zhang, J. Power Sources 196 (2011) 4436–4444.
[12] A.Y. Tonkovich, J.L. Zilka, M.J. LaMont, Y. Wang, R.S. Wegeng, Chem. Eng. Sci. 54 (1999) 2947–2951.
[13] J. Benziger, E. Kimball, R. Mejia-Ariza, I. Kevrekidis, AIChE J. 57 (2010) 2505–2517.
[14] S.A. Freunberger, Y. Chen, Z. Peng, J.M. Griffin, L.J. Hardwick, F. Barde, P. Novak, P.G. Bruce, J. Am. Chem. Soc. 133 (2011) 8040–8047.
[15] V.S. Bryantsev, V. Giordani, W. Walker, M. Blanco, S. Zecevic, K. Sasaki, J. Uddin, D. Addison, G.V. Chase, J. Phys. Chem. A 115 (2011) 12399–12409.
[16] B.D. McCloskey, D.S. Bethune, R.M. Shelby, G. Girishkumar, A.C. Luntz, J. Phys. Chem. Lett. 2 (2011) 1161–1166.
[17] F. Mizuno, K. Takechi, S. Higashi, T. Shiga, T. Shiotsuki, N. Takazawa, Y. Sakurabayashi, S. Okazaki, I. Nitta, T. Kodama, H. Nakamoto, H. Nishikoori, S. Nakanishi, Y. Kotani, H. Iba, J. Power Sources 228 (2013) 47–56.
[18] Z.H. Cui, W.G. Fan, X.X. Guo, J. Power Sources 235 (2013) 251–255.
[19] H.F. Xiang, B. Yin, H. Wang, H.W. Lin, X.W. Ge, S. Xie, C.H. Chen, Electrochim. Acta 55 (2010) 5204–5209.
[20] S. Monaco, A.M. Arangio, F. Soavi, M. Mastragostino, E. Paillard, S. Passerini, Electrochim. Acta 83 (Nov. 2012) 94–104.
[21] M.J. Trahan, S. Mukerjee, E.J. Plichta, M.A. Hendrickson, K.M. Abraham, J. Electrochem. Soc. 160 (2013) A259–A267.
[22] J. Crank, Mathematics of Diffusion, second ed., Oxford University Press, London, 1955, p. 34.
[23] Y. Qiao, F. Yan, S. Xia, S. Yin, P. Ma, J. Chem. Eng. Data 56 (2011) 2379–2385.